Chapter 2

A low-cost, wearable sEMG sensor for upper-limb prosthetic application

2.1 Introduction

Surface Electromyography (sEMG) is a non-invasive technique for the assessment of the myoelectric signal. It is usually preferred because it is painless and quite easy to acquire (Day, 2002). The precise measurement and analysis of sEMG signals are utilized in various applications that include clinical diagnosis of neuromuscular disorders, the study of muscle fatigue, and control of prosthetics. Nowadays, sEMG has been established as a primary source of control for prosthetic hands due to their ease and intuitiveness (Tavakoli, Benussi, and Lourenco 2017; Liu and Zhou 2013; Pancholi and Joshi 2018). A single-channel sEMG is sufficient to detect different activations of upper-limb muscles for numerous applications in rehabilitation and human-computer interface (HCI) (Phinyomark, Phukpattaranont, and Limsakul 2012).

The myoelectric prosthesis is a type of externally powered prosthesis that utilizes EMG signal from an amputee's residual limb to restore their lost capabilities. It mainly consists of a device for capturing EMG signals, a controller for processing these signals, and generating a control command in real-time to drive the actuator mechanically linked with the prosthetics (Parker, Englehart, and Hudgins 2006; Asghari Oskoei and Hu 2007). The operation of smart EMG-based prosthesis, working as an artificial substitute to missing limbs, is affected by numerous factors like change in position of the electrode, variation in muscle contraction, the positioning of the forearm and limb orientation (Khushaba et al. 2016).

A control scheme in myoelectric prosthesis translates the information contained in the EMG signal to control command for the actuation of prosthetic devices. Proportional and threshold schemes are non-pattern recognition-based myoelectric control schemes that rely on factors like characteristics of EMG sensor, data acquisition system, sensor position on the skin,

physiology of muscles and muscle fatigue for proper generation of control commands (Herle et al., 2012; Hudgins, Parker, and Scott 1993). In proportional control, the speed or force of the prosthetic hand is controlled using the intensity of the EMG signal in a proportional manner (Lenzi et al. 2011; Fougner et al. 2012). Such a scheme provides intuitive control and faster-grasping capability to the hand. Although proportional control provides a limited number of prosthetic hand operations, an increased number of grip patterns with accurate force control can be achieved when combined with the pattern recognition approach (Asghari Oskoei and Hu 2007).

Electromyography signals are influenced by several factors, such as the anatomy and physiology of muscles and different noise sources. Inherent noise, motion artifacts, electromagnetic noise, and crosstalk are the most common noise sources present in the EMG signal (Chowdhury et al. 2013). The usual amplitude of raw sEMG signal from forearm muscles lies in the range of 0-10 mV p-p (peak-to-peak), and typically the frequency content ranges between 0-1000 Hz, showing the most relevant information between 10-350 Hz (Day, 2002; Konrad, 2006). A signal conditioning circuitry consisting of amplifiers and filters is required for the reliable detection of such signals. The quality of the myoelectric signal for prosthetic hand control mainly depends on the conditioning circuitry of the sEMG acquisition system (Shobaki et al. 2013). Signal-to-noise ratio (SNR) is a significant parameter that measures the quality of the EMG signal and is estimated statistically by automatic or manual detection of muscular contraction and baseline noise from the signal (DelsysAdmin 2019.; Agostini and Knaflitz 2012).

Modern EMG systems with a large number of features offer a high-quality recording of myoelectric signals. However, the main issues with all these commercial EMG systems are

their extremely high cost, non-portability, complexity, and inability to provide an open-source platform (Supuk, Skelin, and Cic 2014; Imtiaz et al. 2013). Clinical diagnostics requires high-end EMG equipment capable of giving high-quality and multichannel signals. Such devices mainly target offline data analysis. Hence, there is no bar on their response time (Drost et al. 2006). Whereas for prosthetic control, moderate quality EMG device with less response time (below 300 ms) and a high degree of intuitiveness is required (Farina et al. 2014; Farrell and Weir 2007; K. Englehart and Hudgins 2003; Kevin Englehart, Hudgins, and Chan 2003; Chu, Moon, and Mun 2006; Jiang, Lorrain, and Farina 2014; Hakonen, Piitulainen, and Visala 2015; Vujaklija et al. 2018). Moreover, the device should be simple, affordable, and compact enough to fit inside the prosthetic hand socket (Milosevic, Benatti, and Farella 2017). Table 1 describes the technical specifications and cost of some commercially available EMG devices ("Ottobock US Healthcare"; "Myo Armband"; "MyoWare Muscle Sensor"; "Trigno Wireless EMG"; "OYMotion Magic Now"; "Wave Plus Wireless EMG").

This chapter describes the design of a compact-sized sEMG sensor, its validation, and its application for controlling upper-limb prosthesis. The various parameters of the designed sensor, such as amplitude sensitivity, SNR, and response time, were determined and compared with that of a commercial sEMG sensor. Further, the designed sensor was successfully trialed on amputees for controlling a custom-made 3D printed prosthetic hand. The sensor produces output as a linear envelope of 0-5 V proportional to the strength of the EMG signal, which can be easily interfaced with data acquisition devices (DAQ) and microcontrollers for storage and control applications.

	Ottobock 13E200	Myoware muscle sensor	Myo armband	Delsys Trigno Wireless	Oymotion gForce-Pro	Cometa mini Wave
Input	±3 mV	±1.5 mV	±1 mV	±11 mV	±2.5 mV	±2.5 mV
Output type	0-3.3 V envelope	0-5 V envelope, Differential (±2.5 V)	Differential (±2.5 mV)	Differential (±5 V)	Differential (±2.5 V)	Differential (±2.5 V)
Type of electrodes	Stainless steel	Disposable Ag/AgCl	Stainless steel	Silver	Stainless steel (silver-coated)	Silver
Number of channels	1	1	8	16	8	16
Power supply	External	External	Integrated	Integrated	Integrated	Integrated
Weight	4.5 g	9 g	93 g	14.7 g (per channel)	80 g	43 g
Output accessibility	Easily accessible	Easily accessible	Does not provide an open-source platform	Does not provide an open-source platform	Easily accessible	Does not provide an open-source platform
Price	$400	$37.95	$200	$20,000 (for 16 channel)	$150	$15,000 (for 16 channel)

Table 2.1 Commercially available EMG devices.

2.2 Materials and methods

2.2.1 Design and construction of the sensor

The proposed EMG sensor primarily comprises (i) skin interface for assessment of muscle activity under the skin (ii) signal conditioning circuit for converting the raw EMG signal directly from the electrodes to a linear envelope of 0-5 V (iii) a power supply unit for powering the signal conditioning unit, all enclosed in a single package. Figure 2.1 shows the block diagram of the sensor describing its integral parts.

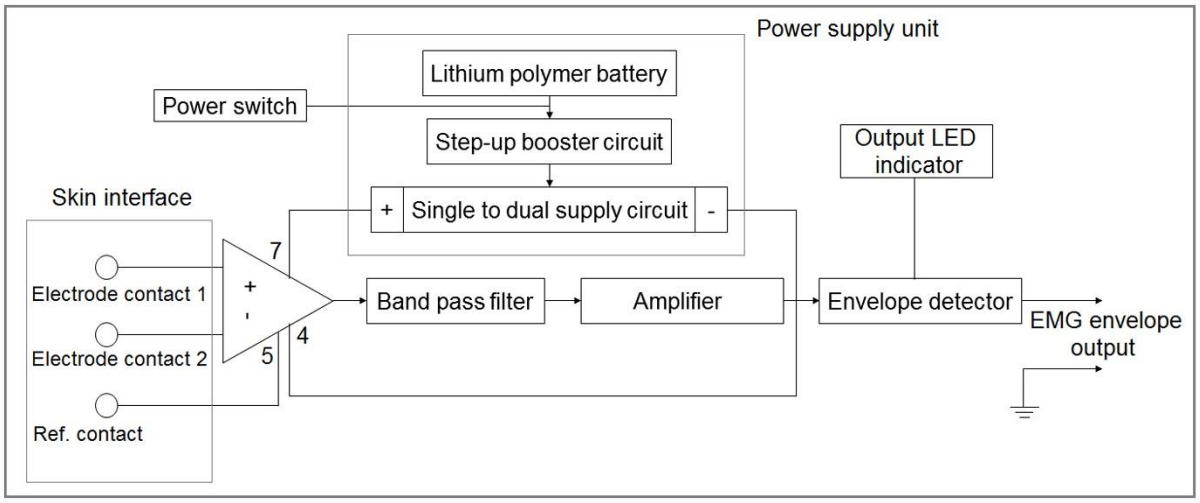

Figure 2.1 Block diagram representation of the proposed EMG sensor.

2.2.1.1 Design of skin interface

Placement of surface electrodes on the skin detects muscle activity in electrical form. The skin interface was designed using three-electrode connectors, out of which two were fixed in the 3D printed sensor chassis, intended for target muscles, while the third one was held free to be used as a reference. Stainless steel buttons were employed here as connectors through which the disposable silver/silver-chloride (Ag/AgCl) electrodes snap directly into the sensor. Figure 3(b) shows the skin interface of the sensor consisting of two electrode snap connectors held at an inter-electrode distance of 4 cm, while the third connector is for connecting the reference electrode. Such an arrangement of electrode connectors minimizes motion artifacts, which usually occur due to the movement of electrode cables (Gerdle et al. 1999).

2.2.1.2 Design of signal conditioning circuitry

Signal boosting, removal of undesired components, and signal translation are the key tasks performed by the signal conditioning unit of the sensor. Figure 2.1 describes the various stages involved in the signal conditioning circuitry.

The preamplifier stage was incorporated using an instrumentation amplifier IC (i.e., INA 128P) with gain adjusted to a lower value of 11.7 to avoid saturation and instability in the output response of successive stages (Wang, Tang, and E Bronlund 2013).

A band-pass filter stage has been added with a lower cut-off frequency of 11 Hz and the higher cut-off frequency of 324 Hz. The gain of the band-pass filter was kept at a value of 3.18 to increase the signal amplitude by some level. This stage was implemented to remove the motion artifacts and external noises of low frequencies and noises occurring at high frequencies. The overall transfer function of the designed band-pass filter is described in equation (2.1).

$$G(s) = \frac{12181528s^2}{(s^2+167s+5201)(s^2+4837s+4137219)} \quad (2.1)$$

A further amplification was provided with a gain of 109.7 to increase the voltage level of the filtered sEMG signal such that storage and control devices can effortlessly access it. The overall gain until this stage has been kept near 3700.

An envelope detector circuit is shown in Figure 2.2(a) was implemented using a half-wave precision rectifier and an RC low-pass filter (Rice, Venkatachalam, and Wegmann 1988). This stage was implemented such that the magnitude of the sEMG signal should remain unaffected by other factors except for the excitation level of the muscles (Farina 2006). The time constant of an RC filter regulates the shape and the speed of the generation of the envelope. For producing a clear envelope of sEMG signal, the time constant of the RC filter should range from 10 ms to 150 ms (D'Alessio and Conforto 2001; Balbinot and Favieiro 2013). A large time constant assures smooth and repeatable envelopes but prevents the detection of short activations, whereas a short time constant shows quick variations in the envelope but reduces the degree of smoothness. Therefore, the time constant was adjusted to a trade-off value of 117

ms by manually tuning the value of R and C considering the output envelope for the prosthetic application (i.e., smooth and a faster envelope) (D'Alessio and Conforto 2001). This stage produces the final output as a 0-5 V linear envelope of the EMG signal, proportional to the level of muscle contraction. A light-emitting diode (LED) was incorporated at the output of the envelope detector, which indicates the captured EMG signal in terms of its glowing intensity.

2.2.1.3 Power supply unit

The main reasons for including power supply unit within the sensor package are: (1) majority of the active components present in the signal conditioning circuitry of the sensor requires a dual power supply for their operation (2) to make the sensor highly compact and wearable (i.e., independent of external power supply which can introduce complexity in acquisition). The power supply unit of the sensor has been equipped with a rechargeable 3.7 V, 240 mAh lithium-polymer battery, a step-up boost converter circuit for increasing the voltage level from the battery (i.e., 3.7 V to 12 V), and a single to dual supply circuit for converting the unipolar output voltage from booster circuit to bipolar supply. The booster circuit primarily incorporates a power MOSFET with fixed switching frequency from automatic pulse frequency modulation. Figure 2.2(b) describes the detailed circuit for the step-up booster and single to dual supply. A single pole double throw (SPDT) slider switch was used to power the sensor, as shown in Figure 2.1.

2.2.1.4 Description of the developed sensor

Figure 2.3(a) describes the front view of the developed sensor showing signal conditioning circuitry and power supply unit, whereas Figure 2.3(b) depicts the rear view of the sensor displaying the skin interface. The integration of electrode connectors, signal conditioning

circuitry, and the power supply unit in a single structure makes the sensor compact and wearable for long time use. The overall dimension of the developed sensor was 35×70 mm^2, which can be further reduced (up to one-fourth of the original dimension) by using small size SMD (surface-mount devices) components and professional tools for fabrication. Based on the component's datasheet, the estimated power consumption of the sensor was 25 mA.

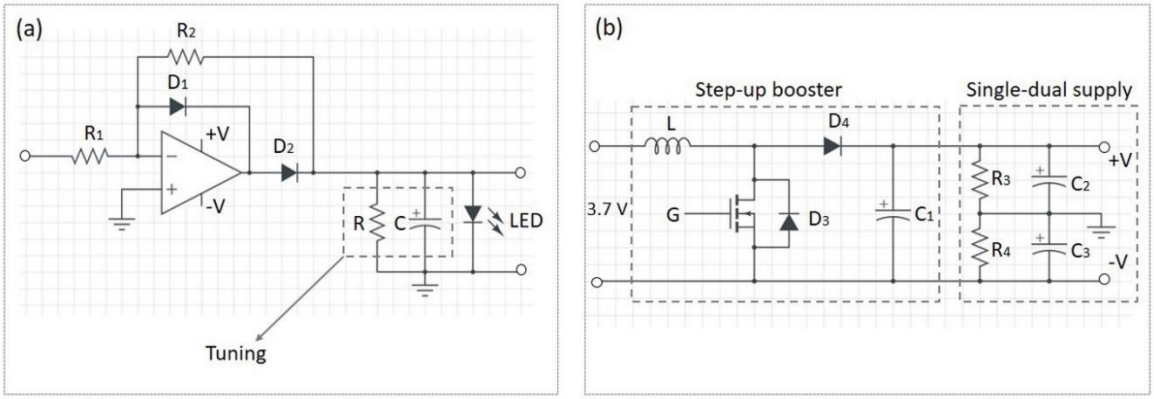

Figure 2.2 (a) Envelope detector circuit, (b) Circuit for step-up booster and single to dual supply.

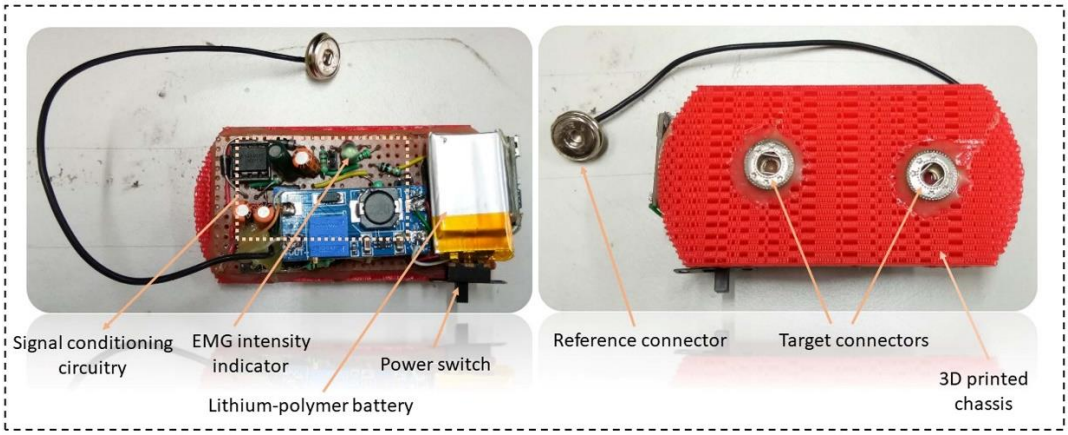

Figure 2.3 (a) Front view of the sensor, (b) Rear view of the sensor showing the skin interface.

2.2.2 Experimental setup for sensor validation

2.2.2.1 Selecting a sensor for comparison

In order to validate the performance of the developed sensor, its output characteristics were compared with that of a commercial EMG sensor. From the specifications mentioned in Table

2.1, it was be observed that Ottobock 13E200 and myoware muscle sensor are the two devices that provide similar nature of output as the developed sensor (i.e., linear envelope). Out of these two devices, myoware muscle sensor was selected for comparison because of its low cost, easy availability, and decent application in prosthesis control (Tavakoli, Benussi, and Lourenco 2017; Pancholi and Joshi 2018; Heywood et al. 2018; Tatarian et al. 2018). EMG data using both sensors were recorded to determine their output parameters.

2.2.2.2 Subject selection

A total of three Amputees and seven healthy subjects participated in EMG data acquisition. Table 2.2 shows the details of each amputee with their type and reason for amputation. Before performing this experiment, ethical clearance was taken by the ethical committee, Institute of medical sciences, BHU, Varanasi.

S.no.	Age	Gender	Weight	Amputation type	Amputation reason
1.	50	Male	85 Kg	Transradial(right hand)	Accident
2.	12	Male	25 Kg	Transradial(right hand)	Accident
3.	20	Male	50 Kg	Transradial(left hand)	Accident

Table 2.2 Details of amputees participated in acquisition.

Subsequently, subjects were asked to sit comfortably on a laboratory chair to record their EMG data. Since amputees cannot perform normal hand activity with their residual limb, maintaining uniformity in EMG data, the same activities (i.e., muscle contraction at different levels) were decided for amputees and healthy subjects acquiring data.

2.2.2.3 Allocating different levels of muscular contraction

Contraction leads to the variation in volume and stiffness of the muscle, which transmits outward forces. These forces can be detected by using force-sensitive resistors (FSRs) placed on the skin in conjunction with a sensitive portion of the muscle. The different levels of contraction were decided based on the force exerted by flexor muscles on the FSR. A highly sensitive band comprising FSR was developed to measure muscular contractile force in terms of voltage. The FSR sensing portion was encased in a 3D printed structure to properly distribute muscular contractile force over the contact surface area. Figure 2.4 shows the sensing area of the designed FSR band, its voltage divider circuit for converting the change in resistance of FSR to voltage output, and its attachment to the forearm for measuring contractile force. Using the force curve of FSR given in the datasheet (FSR-402) and relation in equation (2.2), the different force levels were converted to their corresponding voltage levels, shown in Table 2.3.

$$V_{out} = V_{cc} * \frac{R}{R+R_{FSR}} \tag{2.2}$$

Where V_{cc} is the supply voltage, and its value was selected at 3.7 V, R_{FSR} is the resistance of FSR, R is a fixed resistance of 15 kΩ, and V_{out} is the output voltage of FSR. A force-voltage calibration curve obtained for the FSR is shown in Figure 2.5.

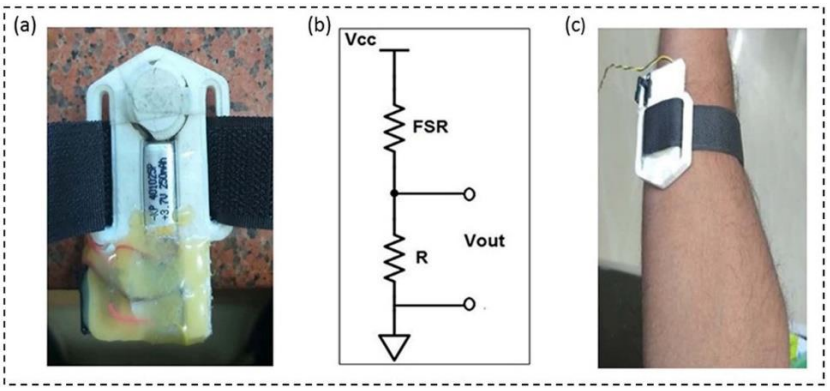

Figure 2.4 (a) Sensing area of the FSR band, (b) Output circuit for the band, (c) Attachment of band to the forearm.

Force (N)	FSR output(V_{out}) (V)	Allocated contraction level
0.156	0.49	-
0.176	0.87	Level 1
0.196	1.25	Level 2
0.294	1.71	Level 3
0.49	2.27	Level 4
0.98	2.84	Level 5
2.51	3.25	Level 6 **(MVC)**
4.9	3.34	-
9.8	3.51	-
19.6	3.60	-

Table 2.3 Contraction level based on FSR output.

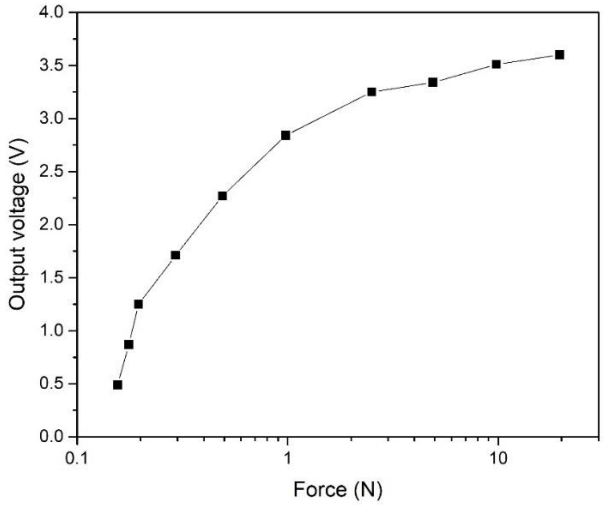

Figure 2.5 Force voltage calibration curve for the FSR band.

For maximum voluntary contraction (MVC) of forearm muscle, the output produced by the FSR band was around 3.2 V similarly, for the minimum contraction of muscle, the output voltage was nearly 0.8 V. Consequently, analyzing the calibrated FSR output in Table 2.3, a

maximum of six levels of muscular contraction were allocated (in Table 2.3) for recording EMG signal where the sixth level corresponds to the MVC of the forearm muscle.

2.2.2.4 Positioning of sensors

The sensors were attached to the forearm stump of amputees and healthy subjects to capture their sEMG signal, as shown in Figure 2.6. The target electrode connectors of the sensors were fixed at flexor carpi radialis and flexor carpi ulnaris muscles via disposable Ag-AgCl (silver-silver chloride) electrodes, while the reference electrode connector was fixed at the elbow portion as these muscle groups on the forearm is directly responsible for the flexion of fingers (Balbinot and Favieiro 2013).

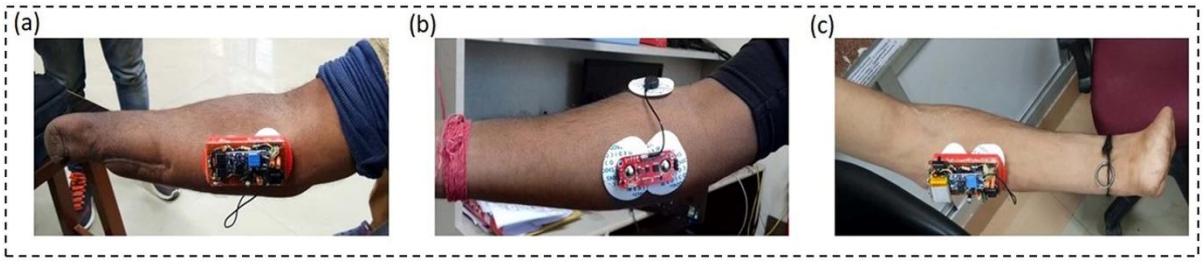

Figure 2.6 Attachment of sensors on the forearm of subjects.

2.2.2.5 Data acquisition

The output of the EMG sensor was connected to the analog input port of NI ELVIS II+ for data acquisition. The EMG data were acquired using Lab VIEW 2015 software interface at a sampling frequency of 2 kS/s.

For recording EMG data, the subjects were asked to perform six different levels of muscular contractions (defined in Table 2.3) of their forearm. Ten repeated readings were recorded for every level. Each recording was conducted for 5 seconds duration.

2.3 Results and discussion

Raw EMG signal (i.e., filtered EMG) and its envelope, obtained by the developed sensor for medium muscle contraction, are illustrated in Figure 2.7. The figure clearly shows that the sensor was capable of generating the envelope of the EMG signal.

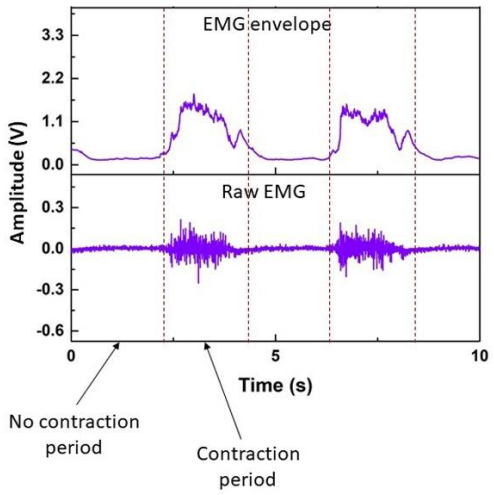

Figure 2.7 Raw EMG and its envelope obtained by the sensor.

Figure 2.8(a) and 2.8(b) show the EMG signal envelopes for six different levels of muscular contractions (i.e., movements) of an amputee acquired with the developed sensor and myoware muscle sensor.

2.3.1 Amplitude analysis

Amplitude analysis of the acquired signals with both sensors was done for movement repetition. Figures 2.9(a) and 2.9(b) show the variability of the EMG signal on the ten repetitions considering all movements (i.e., contractions) and subjects. One way multivariate analysis of variance (MANOVA) was performed using graph pad prism. The study showed no significant differences between the EMG amplitudes for different movement repetitions ($P>0.05$) with both the sensors.

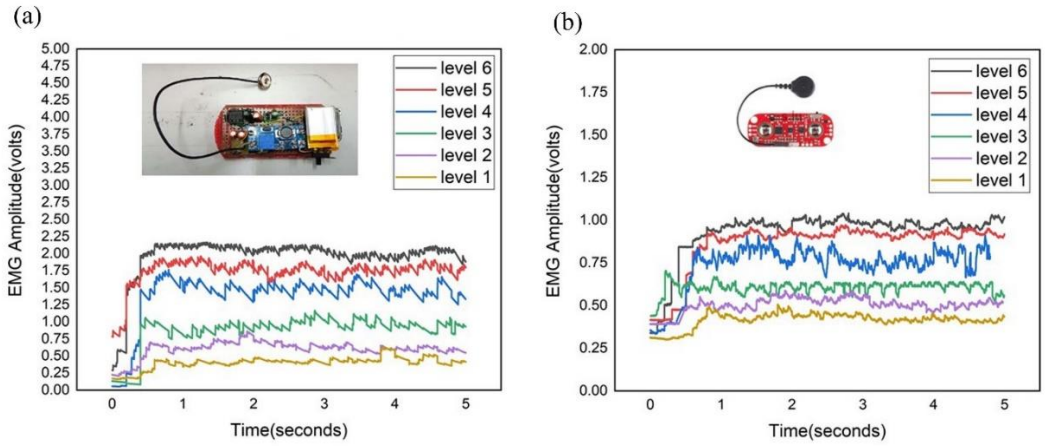

Figure 2.8 Obtained EMG Signal envelopes with (a) Developed sensor, (b) Myoware muscle sensor.

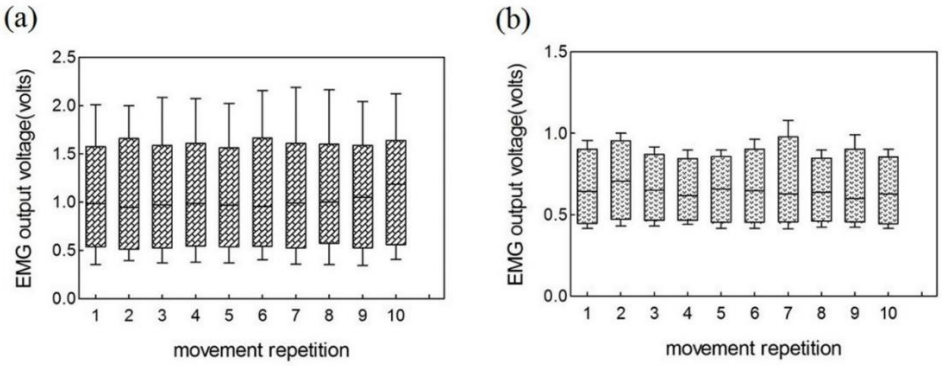

Figure 2.9 EMG output voltage vs. movement repetition for (a) developed sensor (b) myoware sensor.

2.3.2 Signal-to-noise ratio (SNR) calculation

The assessment of the quality of signals produced by the sensor was quantified through the signal-to-noise ratio (SNR) of acquired EMG signals (Konrad, 2006). For this, 5 seconds of data samples were recorded using both the sensors for two conditions: (i) when there was no muscle contraction. Here, the root mean square (RMS) value of the captured signals gave the total noise level of the sensor (ii) when maximum voluntary contraction (MVC) was made. The RMS value of acquired signals provides the signal strength of the sensor. Figure 2.10 shows the waveform indicating noise level (baseline noise) and signal strength for a subject

using the developed sensor. The SNR values for both the sensors were evaluated using the equation (2.3), considering each subject.

$$SNR = 20\ log_{10}\left(\frac{RMS_{signal}}{RMS_{noise}}\right) \tag{2.3}$$

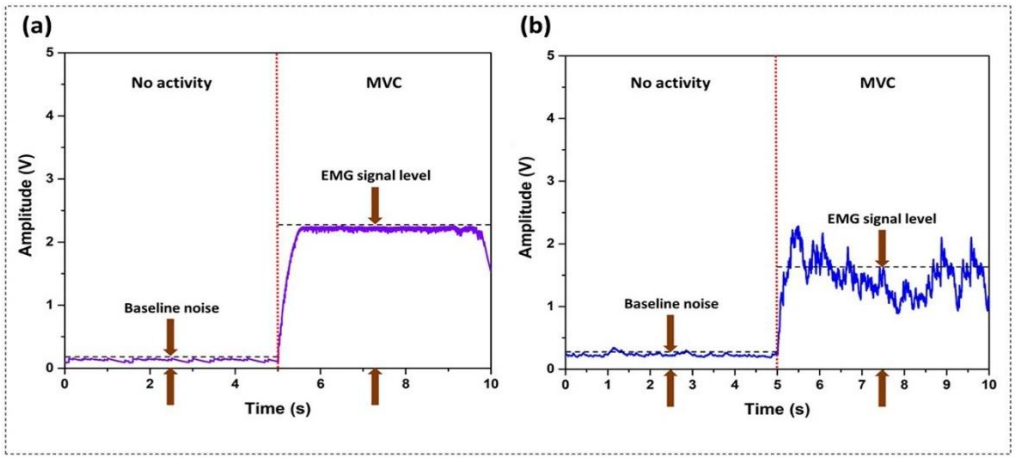

Figure 2.10 Noise level and EMG signal level obtained using (a) developed sensor, (b) commercial sensor.

Table 2.4 shows the average RMS values (with deviations) from contractions and obtained values of SNR for sensors. The results in this table indicate the higher SNR values of the proposed sensor compared to the commercial sensor. Although the contractile force is the same for each subject, the resultant RMS value is different due to variations in muscle strength, muscle geometry, tissue filter, and electrode-skin interface (Laferriere, Lemaire, and Chan 2011).

Subject	Sensor	SNR (dB)
1	developed	33.1
	myoware	23.1
2	developed	31.5
	myoware	22.5
3	developed	32.6
	myoware	22.8

4	developed	30.8
	myoware	21.1
5	developed	31.9
	myoware	22.2
6	developed	32.2
	myoware	23.5
7	developed	33.6
	myoware	24.1
8	developed	33.8
	myoware	23.6
9	developed	33.2
	myoware	23.8
10	developed	34.1
	myoware	24.3
Average value	developed	32.68
	myoware	23.1

Table 2.4 Determined SNR by sensor type.

2.3.3 Sensitivity analysis

Amplitude sensitivity was determined as the ratio of incremental change in the sensor's output voltage to the variation in the muscular contraction level (i.e., input to the EMG sensor). Figure 2.11(a) and 2.11(b) show the difference of EMG output voltage as a function of six specified muscular contraction levels with both the sensors for (i) all the subjects (ii) only amputees. The slope of the linear curves for both cases was computed to give the sensitivities for the sensors. Results indicated the higher sensitivity of the developed sensor (70% higher in the case for only amputees and 50% higher in the case for all the subjects) than the myoware sensor.

Sensitivities of both the sensors were determined at their fixed gain, at which their SNR is maximum. Because as we increase the gain of an EMG system above a certain value, its baseline noise increases, which decreases the SNR value of the system (Agostini and Knaflitz 2012).

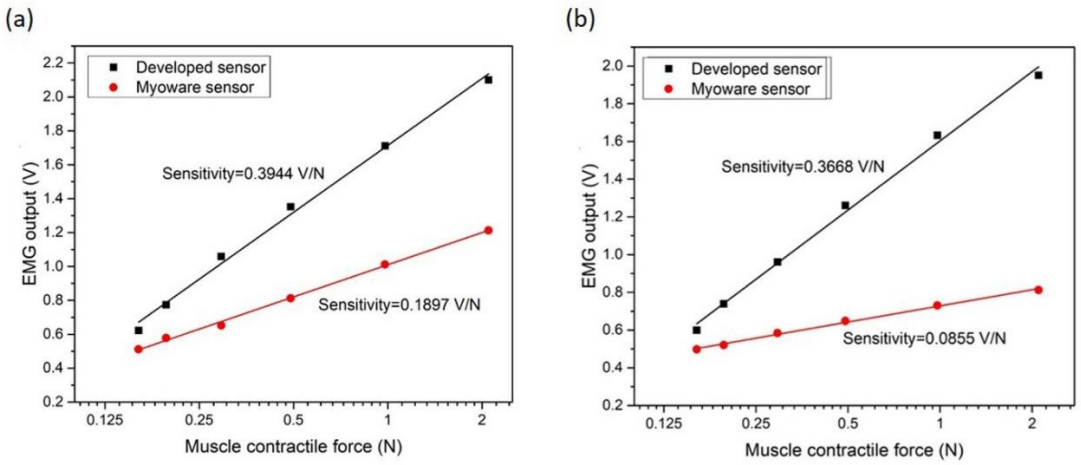

Figure 2.11 (a) Sensitivity comparison of sensors for all the subjects, (b) Sensitivity comparison of sensors for amputees.

2.3.4 Response time analysis

Rise and fall time were determined from all the real-time generated EMG envelopes with both the sensors for all the six levels of muscular contractions (defined in Table 2.3) considering each subject. Figure 2.12 shows the calculation of rise and fall time from the EMG envelope obtained for the medium contraction level of muscles with the developed sensor. In Table 2.5, the first six rows indicate the average rise and fall time calculated for each contraction level considering all the subjects, while the last row gives the sensors' overall rise and fall time. The rise time for the developed sensor was obtained to be 57 % faster (lower) than the myoware sensor, whereas fall time for the sensor was observed 53 % higher than the commercial sensor. Tuning of RC parameters in the envelope detection stage was mainly responsible for generating such an envelope (i.e., lower rise time and higher fall time).

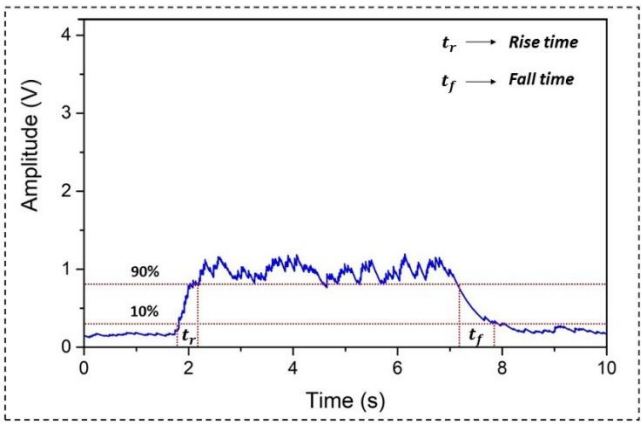

Figure 2.12 Rise and fall time calculation from the envelope produced with the developed sensor.

Muscular contraction level	Rise time, t_r (ms)		Fall time, t_f (ms)	
	Myoware	**Developed sensor**	**Myoware**	**Developed sensor**
1	260	110	190	360
2	280	110	220	390
3	310	130	230	410
4	340	140	270	450
5	370	160	310	490
6	380	170	350	540
Average	323	136	261	440

Table 2.5 Rise and fall time for the sensors.

2.4 Sensor application for controlling a prosthetic hand

2.4.1 Development of prosthetic hand prototype

E-NABLE Phoenix Hand v2 was printed using a 3D printer, which is an open-source hand model available at Thingiverse website ("E-NABLE Phoenix Hand v2"). An extrinsic actuation scheme was implemented for the hand prototype using two servomotors, i.e., actuators located outside the hand (Kargov et al. 2004). High-torque metal-geared servomotor

(MG-995) was used here as an actuator providing maximum torque up to 10 Kgf.cm at an operating voltage of 5 V. Each finger of the hand was equipped with a silicon fingertip for enhancing the grasping capability. Figure 2.13 shows the developed 3D printed hand prototype.

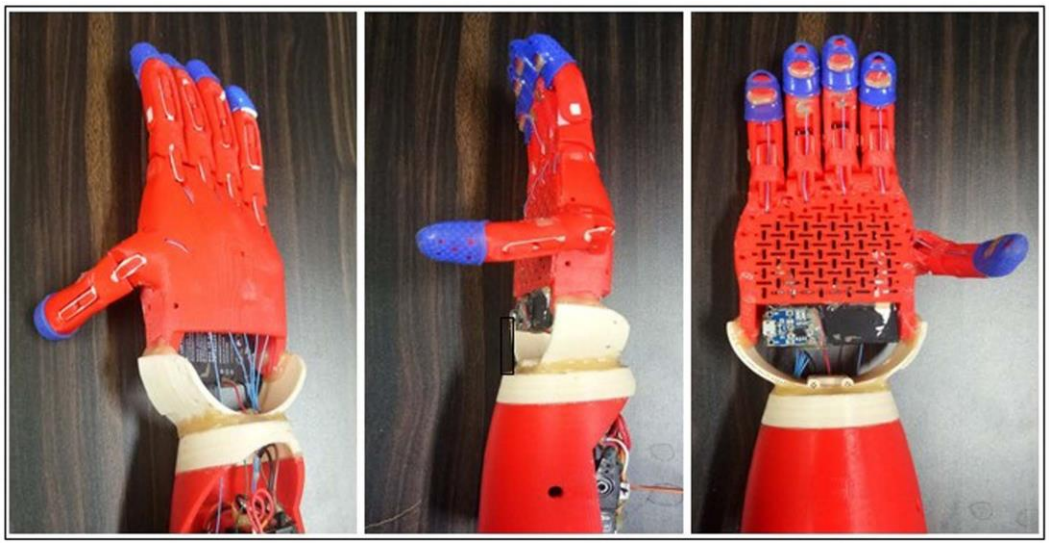

Figure 2.13 Prepared 3D printed hand prototype.

2.4.2 Implementation of a control strategy for the generation of control command using the EMG signal from the sensor

The proportional control strategy was implemented, translating the 0-5 V EMG information from the sensor to pulse width modulation (PWM) signal in real-time for driving the servomotor actuating the prosthetic hand. A PWM signal is a digital control signal consisting of two main components that describe its behaviour, i.e., a duty cycle and a frequency. Here, the duty cycle of the PWM signal was varied proportionally with the mean absolute value (MAV) of the EMG signal. This strategy was realized on the microcontroller chip (i.e., Arduino Nano) using the Arduino software platform. Figure 2.14 shows the schematic for the generation of the control command to drive a prosthetic hand.

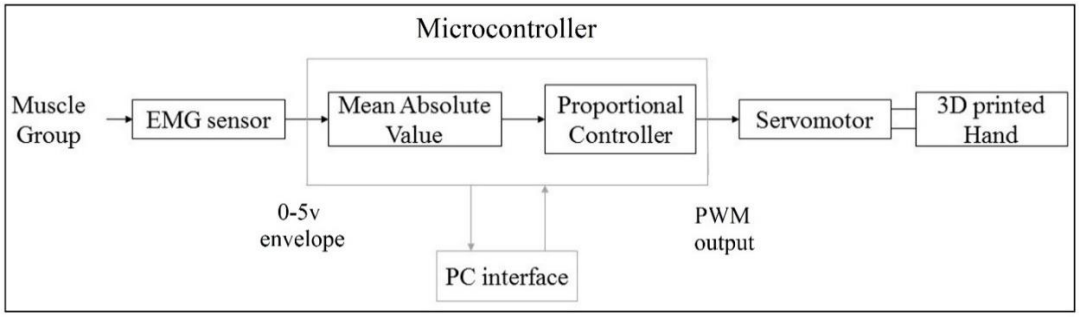

Figure 2.14 Schematic for generating the control command.

The proportional myoelectric control scheme here allows the grasping force of prosthetic hand fingers proportional to the strength of the EMG signal, i.e., the higher the intensity of the EMG signal tighter will be the closing of hand fingers.

2.4.3 Utilization of the sensor on amputees to control the operation of the prosthetic hand

The sensor was attached to the residual forearm stump of amputees for the real-time operation of the prosthetic hand. Amputees with their different levels of muscular contraction (intensity of sEMG signal) were able to control the grasping force of the prosthetic hand fingers to grab and hold various shaped objects without any prior training. Figure 2.15 shows the various grasping operations performed by the prosthetic hand using EMG signals from amputees.

Response time (i.e., Closing/opening time) of the prosthetic hand with both the sensors were determined from the recorded video of hand operation. Table 2.6 provides the closing and opening time of prosthetic hand fingers with both sensors. From the observations in Tables 2.5 and 2.6, it was established that the rise and fall time of the generated envelope, i.e., the response time of the EMG sensor, mainly regulates the closing and opening time of the prosthetic hand fingers.

The prosthetic hand with the designed sensor showed better response time as compared to the myoware sensor. Furthermore, the response time of the prosthetic hand with the designed sensor was found to be comparable to the response time of the ottobock sensor hand (i.e., the closing/opening time of 300/300 ms), which is regarded as one of the fastest commercially available myoelectric hands ("Myoelectric Speed Hands").

Figure 2.15 Performed operations by prosthetic hand using sEMG signal from amputees.

Prosthetic hand	Closing time (ms)	Opening time (ms)
With developed sensor	350	650
With myoware muscle sensor	550	450

Table 2.6 The response time of hand with both the sensors.

2.5 Conclusion

In this chapter, a low-cost and wearable sEMG sensor was designed for upper-limb prosthetic application. The presence of a skin interface, pre-processing circuitry, and power supply unit within the same structure makes the sensor's construction highly compact and portable.

The designed sensor showed better performance characteristics, i.e., very high SNR values, higher amplitude sensitivity, and faster response time than the commercial sensor. A detailed comparison between both the sensors is provided in Table 2.7.

	Myoware muscle sensor	**Developed EMG sensor**
Operating voltage	3.1-5 V	1.5-6 V
Power supply	External	Integrated
Power consumption	9 mA	25 mA
Mass	9 g	45 g
Dimension	20×50 mm^2	35×70 mm^2
Rise time	323 ms	136 ms
Fall time	261 ms	440 ms
Sensitivity	0.18973 V/N	0.3944 V/N
SNR	23.10 dB	32.68 dB
Price in the commercial market	$37.95	Prototyping cost($13)

Table 2.7 Comparison table for the sensors.

Further, the developed sensor was evaluated for prosthetic hand control using EMG signals from amputees. The proportional control scheme enables the amputees to control the grasping force of prosthetic hand fingers with their EMG signals. The higher sensitivity, along with the increased SNR feature for this sensing system, enables reliable detection of EMG signal regardless of subject variability and results in the smooth operation of the prosthetic hand. On the other hand, the sensor's response time regulates the actuation speed of the prosthetic hand. The lower rise time of the sensor provides faster closing of prosthetic hand fingers to grasp the objects (when the muscle is contracted), whereas higher fall time offers delay in the opening of hand fingers to prevent immediate release (i.e., slippage) of grasped objects(when the

muscle is instantly relaxed). The tuning of RC parameters in the envelope detection stage of the sensor was mainly responsible for the generation of a smoother envelope with lower rise time and higher fall time. The sensor realized with proportional control to deliver smooth and faster actuation of the prosthetic hand with control on grasp force. Moreover, the prosthetic hand prototype with the designed sensor and implemented control strategy displayed comparable response time to the commercial ottobock sensor hand.

Larger size and mass are issues with the designed sensor, which can be easily resolved using miniature-sized SMD components and professional tools for fabrication. However, with improved parameters and reduced size, the sensor can make a real clinical difference to be used by amputees for controlling prostheses. One more limitation with the designed sensor is that it requires disposable Ag/Agcl electrodes whose performance degrades with time. This drawback can be settled by redesigning the sensor with high-quality dry electrodes as a skin interface.

For future work, the EMG signals acquired with the sensor for the different levels of muscular contraction can be classified to achieve individual finger movement of the prosthetic hand. Also, such an unsophisticated, effective, and low-cost sensor can be utilized to develop an affordable myoelectric hand.

2.6 References

Agostini, V., and M. Knaflitz. 2012. "An Algorithm for the Estimation of the Signal-To-Noise Ratio in Surface Myoelectric Signals Generated During Cyclic Movements." IEEE Transactions on Biomedical Engineering 59 (1): 219–25. https://doi.org/10.1109/TBME.2011.2170687.

Asghari Oskoei, Mohammadreza, and Huosheng Hu. 2007. "Myoelectric Control Systems—A Survey." Biomedical Signal Processing and Control 2 (4): 275–94. https://doi.org/10.1016/j.bspc.2007.07.009.

Balbinot, Alexandre, and Gabriela Favieiro. 2013. "A Neuro-Fuzzy System for Characterization of Arm Movements." Sensors (Basel, Switzerland) 13 (2): 2613–30. https://doi.org/10.3390/s130202613.

Chowdhury, Rubana H., Mamun B. I. Reaz, Mohd Alauddin Bin Mohd Ali, Ashrif A. A. Bakar, Kalaivani Chellappan, and Tae G. Chang. 2013. "Surface Electromyography Signal Processing and Classification Techniques." Sensors 13 (9): 12431–66. https://doi.org/10.3390/s130912431.

Chu, J.-, I. Moon, and M.- Mun. 2006. "A Real-Time EMG Pattern Recognition System Based on Linear-Nonlinear Feature Projection for a Multifunction Myoelectric Hand." IEEE Transactions on Biomedical Engineering 53 (11): 2232–39. https://doi.org/10.1109/TBME.2006.883695.

D'Alessio, T., and S. Conforto. 2001. "Extraction of the Envelope from Surface EMG Signals." IEEE Engineering in Medicine and Biology Magazine 20 (6): 55–61. https://doi.org/10.1109/51.982276.

Day, Scott. 2002 "Important factors in surface EMG measurement," Calgary, AB: Bortec Biomedical Ltd Publishers.

DelsysAdmin. n.d. "What Factors Affect EMG Signal Quality?" Delsys, Inc. (blog). Accessed January 28, 2019. https://www.delsys.com/products/software/emgworks/sqm/factors/.

Drost, Gea, Dick F. Stegeman, Baziel G. M. van Engelen, and Machiel J. Zwarts. 2006. "Clinical Applications of High-Density Surface EMG: A Systematic Review." Journal of Electromyography and Kinesiology: Official Journal of the International Society of Electrophysiological Kinesiology 16 (6): 586–602. https://doi.org/10.1016/j.jelekin.2006.09.005.

"Electrode | Electrodes | Myo Control Elements | Myo Hands and Components | Upper Limb Prosthetics | Prosthetics | Ottobock US Healthcare." n.d. Accessed December 4, 2018. https://professionals.ottobockus.com/Prosthetics/Upper-Limb-Prosthetics/Myo-Hands-and-Components/Myo-Control-Elements/Electrodes/Electrode/p/13E200~560.

"E-NABLE Phoenix Hand v2 by EnableCommunityFoundation - Thingiverse." 2015. Accessed January 28, 2019. https://www.thingiverse.com/thing:1453190.

Englehart, K., and B. Hudgins. 2003. "A Robust, Real-Time Control Scheme for Multifunction Myoelectric Control." IEEE Transactions on Biomedical Engineering 50 (7): 848–54. https://doi.org/10.1109/TBME.2003.813539.

Englehart, Kevin, Bernard Hudgins, and Adrian D.C. Chan. 2003. "Continuous Multifunction Myoelectric Control Using Pattern Recognition." Edited by Peter Kyberd, Paul Chappell, and David Gow. Technology and Disability 15 (2): 95–103. https://doi.org/10.3233/TAD-2003-15205.

Farina, Dario. 2006. “Interpretation of the Surface Electromyogram in Dynamic Contractions.” Exercise and Sport Sciences Reviews 34 (3): 121–27.

Farina, Dario, Ning Jiang, Hubertus Rehbaum, Ales Holobar, Bernhard Graimann, Hans Dietl, and Oskar C. Aszmann. 2014. “The Extraction of Neural Information from the Surface EMG for the Control of Upper-Limb Prostheses: Emerging Avenues and Challenges.” IEEE Transactions on Neural Systems and Rehabilitation Engineering 22 (4): 797–809. https://doi.org/10.1109/TNSRE.2014.2305111.

Farrell, Todd R., and Richard F. Weir. 2007. “The Optimal Controller Delay for Myoelectric Prostheses.” IEEE Transactions on Neural Systems and Rehabilitation Engineering: A Publication of the IEEE Engineering in Medicine and Biology Society 15 (1): 111–18. https://doi.org/10.1109/TNSRE.2007.891391.

Fougner, Anders, Oyvind Stavdahl, Peter J. Kyberd, Yves G. Losier, and Philip A. Parker. 2012. “Control of Upper Limb Prostheses: Terminology and Proportional Myoelectric Control-a Review.” IEEE Transactions on Neural Systems and Rehabilitation Engineering: A Publication of the IEEE Engineering in Medicine and Biology Society 20 (5): 663–77. https://doi.org/10.1109/TNSRE.2012.2196711.

Gerdle, Björn, Stefan Karlsson, Scott Day, and Mats Djupsjöbacka. 1999. “Acquisition, Processing and Analysis of the Surface Electromyogram.” In Modern Techniques in Neuroscience Research, edited by Uwe Windhorst and Håkan Johansson, 705–55. Berlin, Heidelberg: Springer Berlin Heidelberg. https://doi.org/10.1007/978-3-642-58552-4_26.

Hakonen, Maria, Harri Piitulainen, and Arto Visala. 2015. “Current State of Digital Signal Processing in Myoelectric Interfaces and Related Applications.” Biomedical Signal Processing and Control 18 (April): 334–59. https://doi.org/10.1016/j.bspc.2015.02.009.

Herle, Sorin, Sergiu Man, Gheorghe Lazea, and Paula Raica. n.d. “Myoelectric Control Strategies for a Human Upper Limb Prosthesis.” CONTROL ENGINEERING AND APPLIED INFORMATICS, 10.

Heywood, Sophie, Yong Hao Pua, Jodie McClelland, Paula Geigle, Ann Rahmann, Kelly Bower, and Ross Clark. 2018. “Low-Cost Electromyography – Validation against a Commercial System Using Both Manual and Automated Activation Timing Thresholds.” Journal of Electromyography and Kinesiology 42 (October): 74–80. https://doi.org/10.1016/j.jelekin.2018.05.010.

Hudgins, B., P. Parker, and R.N. Scott. 1993. “A New Strategy for Multifunction Myoelectric Control.” IEEE Transactions on Biomedical Engineering 40 (1): 82–94. https://doi.org/10.1109/10.204774.

Imtiaz, U., L. Bartolomeo, Z. Lin, S. Sessa, H. Ishii, K. Saito, M. Zecca, and A. Takanishi. 2013. “Design of a Wireless Miniature Low Cost EMG Sensor Using Gold Plated Dry Electrodes for Biomechanics Research.” In 2013 IEEE International Conference on Mechatronics and Automation, 957–62. https://doi.org/10.1109/ICMA.2013.6618044.

Jiang, Ning, Thomas Lorrain, and Dario Farina. 2014. “A State-Based, Proportional Myoelectric Control Method: Online Validation and Comparison with the Clinical State-of-the-Art.” Journal of NeuroEngineering and Rehabilitation 11 (1): 110. https://doi.org/10.1186/1743-0003-11-110.

Kargov, Artem, Christian Pylatiuk, Jan Martin, Stefan Schulz, and Leonhard Döderlein. 2004. “A Comparison of the Grip Force Distribution in Natural Hands and in Prosthetic

Hands." Disability and Rehabilitation 26 (12): 705–11. https://doi.org/10.1080/09638280410001704278.
Khushaba, Rami N., Ali Al-Timemy, Sarath Kodagoda, and Kianoush Nazarpour. 2016. "Combined Influence of Forearm Orientation and Muscular Contraction on EMG Pattern Recognition." Expert Systems with Applications 61 (November): 154–61. https://doi.org/10.1016/j.eswa.2016.05.031.
Konrad, Peter. 2006 "A Practical Introduction to Kinesiological Electromyography," 61.
Laferriere, Pascal, Edward D. Lemaire, and Adrian D. C. Chan. 2011. "Surface Electromyographic Signals Using Dry Electrodes." IEEE Transactions on Instrumentation and Measurement 60 (10): 3259–68. https://doi.org/10.1109/TIM.2011.2164279.
Lenzi, T., S. M. M. De Rossi, N. Vitiello, and M. C. Carrozza. 2011. "Proportional EMG Control for Upper-Limb Powered Exoskeletons." In 2011 Annual International Conference of the IEEE Engineering in Medicine and Biology Society, 628–31. Boston, MA: IEEE. https://doi.org/10.1109/IEMBS.2011.6090139.
Liu, Jie, and Ping Zhou. 2013. "A Novel Myoelectric Pattern Recognition Strategy for Hand Function Restoration after Incomplete Cervical Spinal Cord Injury." IEEE Transactions on Neural Systems and Rehabilitation Engineering: A Publication of the IEEE Engineering in Medicine and Biology Society 21 (1): 96–103. https://doi.org/10.1109/TNSRE.2012.2218832.
Milosevic, B., S. Benatti, and E. Farella. 2017. "Design Challenges for Wearable EMG Applications." In Design, Automation Test in Europe Conference Exhibition (DATE), 2017, 1432–37. https://doi.org/10.23919/DATE.2017.7927217.
"Myoelectric Speed Hands." 2014. Accessed April 12, 2019. https://www.ottobockus.com/prosthetics/upper-limb-prosthetics/solution-overview/myoelectric-devices-speedhands/.
"MyoWare Muscle Sensor - SEN-13723 - SparkFun Electronics." 2016. Accessed December 4, 2018. https://www.sparkfun.com/products/13723.
"OYMotion Magic Now." 2017. Accessed July 20, 2019. http://www.oymotion.com/site/.
Pancholi, S., and A. M. Joshi. 2018. "Portable EMG Data Acquisition Module for Upper Limb Prosthesis Application." IEEE Sensors Journal 18 (8): 3436–43. https://doi.org/10.1109/JSEN.2018.2809458.
Parker, P., K. Englehart, and B. Hudgins. 2006. "Myoelectric Signal Processing for Control of Powered Limb Prostheses." Journal of Electromyography and Kinesiology: Official Journal of the International Society of Electrophysiological Kinesiology 16 (6): 541–48. https://doi.org/10.1016/j.jelekin.2006.08.006.
Phinyomark, Angkoon, Pornchai Phukpattaranont, and Chusak Limsakul. 2012. "Fractal Analysis Features for Weak and Single-Channel Upper-Limb EMG Signals." Expert Systems with Applications 39 (12): 11156–63. https://doi.org/10.1016/j.eswa.2012.03.039.
Rice, D. A., V. Venkatachalam, and M. J. Wegmann. 1988. "A Simple Envelope Detector." IEEE Transactions on Instrumentation and Measurement 37 (2): 223–26. https://doi.org/10.1109/19.6056.
Shobaki, Mohammed M, Noreha Abdul Malik, Sheroz Khan, Anis Nurashikin, Samnan Haider, Sofiane Larbani, Atika Arshad, and Rumana Tasnim. 2013. "High Quality Acquisition of Surface Electromyography – Conditioning Circuit Design." IOP

Conference Series: Materials Science and Engineering 53 (December): 012027. https://doi.org/10.1088/1757-899X/53/1/012027.

Supuk, Tamara Grujic, Ana Kuzmanic Skelin, and Maja Cic. 2014. “Design, Development and Testing of a Low-Cost SEMG System and Its Use in Recording Muscle Activity in Human Gait.” Sensors (Basel, Switzerland) 14 (5): 8235–58. https://doi.org/10.3390/s140508235.

Tatarian, Karen, Micael S. Couceiro, Eduardo P. Ribeiro, and Diego R. Faria. 2018. “Stepping-Stones to Transhumanism: An EMG-Controlled Low-Cost Prosthetic Hand for Academia.” In 2018 International Conference on Intelligent Systems (IS), 807–12. Funchal - Madeira, Portugal: IEEE. https://doi.org/10.1109/IS.2018.8710489.

Tavakoli, Mahmoud, Carlo Benussi, and Joao Luis Lourenco. 2017. “Single Channel Surface EMG Control of Advanced Prosthetic Hands.” Expert Syst. Appl. 79 (C): 322–332. https://doi.org/10.1016/j.eswa.2017.03.012.

“Trigno Lab | Wireless EMG System.” 2016 Accessed January 28, 2019. https://www.delsys.com/products/wireless-emg/trigno-lab/.

“Using the Armband Manager in Myo Connect.” 2015 Welcome to Myo Support. Accessed January 28, 2019. http://support.getmyo.com/hc/en-us/articles/205031939-Using-the-Armband-Manager-in-Myo-Connect.

Vujaklija, Ivan, Vahid Shalchyan, Ernest N. Kamavuako, Ning Jiang, Hamid R. Marateb, and Dario Farina. 2018. “Online Mapping of EMG Signals into Kinematics by Autoencoding.” Journal of NeuroEngineering and Rehabilitation 15 (1): 21. https://doi.org/10.1186/s12984-018-0363-1.

Wang, Jingpeng, Liqiong Tang, and John E Bronlund. 2013. “Surface EMG Signal Amplification and Filtering.” International Journal of Computer Applications 82 (1): 15–22. https://doi.org/10.5120/14079-2073.

“Wave Plus Wireless EMG.” 2015. Cometa Systems. July 8, 2015. https://www.cometasystems.com/products/wave-plus-wireless-emg.